Electrochimica Acta 109 (2013) 710–715

Contents lists available at ScienceDirect

Electrochimica Acta

journal homepage: www.elsevier.com/locate/electacta

Photoelectrochemical properties of doped lanthanum orthoferrites

Isabella Natali Sora [a,*], Francesca Fontana [a], Rosalba Passalacqua [b], Claudio Ampelli [b], Siglinda Perathoner [b], Gabriele Centi [b], Francesco Parrino [c], Leonardo Palmisano [c]

[a] INSTM R.U. Bergamo and Dipartimento di Ingegneria, University of Bergamo, viale Marconi 5, Dalmine, BG I-24044, Italy
[b] INSTM/CASPE R.U. and Dipartimento di Ingegneria Elettronica, Chimica ed Ingegneria Industriale (DIECII), University of Messina, viale F. Stagno d'Alcontres 31, ME I-98166, Italy
[c] "Schiavello-Grillone" Photocatalysis Group, Dipartimento di Energia, Ingegneria dell'Informazione e Modelli Matematici (DEIM), University of Palermo, Viale delle Scienze, 90128 Palermo, Italy

ARTICLE INFO

Article history:
Received 9 April 2013
Received in revised form 15 July 2013
Accepted 15 July 2013
Available online 31 July 2013

This paper is dedicated to professor Tullio Caronna for his retirement.

Keywords:
Photocatalysts
Photocurrent response
Quasi-Fermi level
Ferrites

ABSTRACT

$LaFeO_3$ powders doped with Sr (20 mol%) and Cu (0-10-20 mol%) were prepared by citrate auto-combustion synthesis and investigated in terms of crystal structure, morphology, surface area and optical properties. All powders showed photocurrent response in the form of a pasted and annealed electrode and as slurry electrode; the highest value was obtained for undoped orthoferrite calcined at 600 °C. Their physical–chemical properties were related to photoelectrochemical behaviour. The position of the quasi-Fermi level of electrons for all the photocatalysts calcined in the range 600–980 °C is about the same within experimental error (between −0.62 and −0.67 V with respect to Ag/AgCl reference electrode, at pH 7). Doping with 20 mol% of strontium did not influence the flat band potential of the powders, while doping with copper caused an important and reproducible change in the titration curve, indicating the presence of intermediate energy states in the samples calcined at 600 °C, but not in those calcined at 980 °C.

1. Introduction

Recently, perovskite-type transition metal oxides (TMOs) have been proposed as promising photocatalysts for wastewater and air pollution treatments [1–5]. Some perovskite-type TMOs are semiconductors with a band gap narrow enough for efficient absorption of visible light, and thus can potentially be employed as visible-light-active photocatalysts. In this case they offer a strong advantage over the most used photocatalyst for environmental remediation, i.e. titanium dioxide, which absorbs UV light, the use of solar radiation or visible-light lamps, and hence the development of lower costs technologies.

Lanthanum orthoferrite $LaFeO_3$, with perovskite structure, exhibits *p*-type conductivity at high oxygen partial pressures ($p_{O2} > 10^{-4}$ atm) [6]. $LaFeO_3$ is a charge-transfer-type insulator and exhibits a band-gap energy of about 2.1–2.0 eV [7,8]. Generally, the functional properties of perovskite materials can be controlled either by modulating structure and defectivity or by substitution of the metal in the oxide. On substituting Sr^{2+} for La^{3+}, hole states with *p* character are introduced in the system above the Fermi level [8], and a band-gap energy at the Fermi level is present for all compositions in the range $0 < x < 0.67$ as shown by the photoemission study reported in Ref. [9]. While most of the photoelectrochemical properties of strontium-doped $LaFeO_3$ are understood, less is known about the effects of simultaneous substitution of iron with copper.

Copper-doped $LaFeO_3$ is a viable candidate as visible-light photocatalytic material, however most of the technical requirements (large specific surface area, high photocatalytic activity, chemical stability, structural integrity, etc.) have not been sufficiently investigated. As a part of an ongoing study on $(La_{1-x}A_x)(Fe_{1-y}B_y)O_3$ perovskites [10–13], several strontium and copper-doped $LaFeO_3$ powders were investigated by photo-electrochemical measurements in order to study their electronic features. The work presented here concerns also their physico-chemical characterization.

2. Experimental

2.1. Synthesis of materials and characterization

$LaFeO_3$ (LF), $La_{0.8}Sr_{0.2}FeO_{3-w}$ (LSF20), $La_{0.8}Sr_{0.2}Fe_{0.9}Cu_{0.1}O_{3-w}$ (LSFC2010) and $La_{0.8}Sr_{0.2}Fe_{0.8}Cu_{0.2}O_{3-w}$ (LSFC2020) powders were prepared by citrate auto-combustion of dry gel obtained from a solution of the corresponding nitrates in citric acid solution. Analytical grade La_2O_3, $Sr(NO_3)_2$, $Fe(NO_3)_3{\cdot}9H_2O$, $Cu(NO_3)_2{\cdot}2.5H_2O$, citric

* Corresponding author. Tel.: +39 035 2052012; fax: +39 035 2052310.
E-mail address: isabella.natali-sora@unibg.it (I. Natali Sora).

0013-4686/$ – see front matter © 2013 Elsevier Ltd. All rights reserved.
http://dx.doi.org/10.1016/j.electacta.2013.07.132

acid, nitric acid, and aqueous NH_3 were used as the starting materials. A specific amount of dried La_2O_3 was dissolved in a nitric acid solution to prepare $La(NO_3)_3{\cdot}6H_2O$. The experimental details have been previously reported [10,11]. The resulting lightweight powder was calcined at 600–980 °C for 3 h in air.

Powder X-ray diffraction patterns (XRD) were collected at room temperature (Cu-Kα radiation). The structural refinements were carried out with the Rietveld method of profile analysis for LSF20, LSFC2010 and LSFC2020 calcined at 600 °C. The morphology of the particles was observed at 20,000× magnification by analytical environmental scanning electron microscopy (LEO 1450EP) at 15 kV. The BET surface area was obtained by nitrogen adsorption–desorption isotherms according to the conventional BET method using a Micromeritics ASAP 2010 system. Powder samples of the photocatalysts were characterized by ultraviolet–visible diffuse reflectance spectroscopy (UV–vis DRS). The spectra were recorded in air with a spectrophotometer UV/VIS/NIR Jasco V-570 equipped with an integrating sphere for solid samples (model ISN-470) in the region 200–2000 nm, $BaSO_4$ was used as reference for the baseline. The reflectance spectra were represented by using the Kubelka–Munk function $F(R_\infty)$ which is proportional to the absorption coefficient obtained for weakly absorbing sample.

2.2. Electrochemical measurements

Photocurrent measurements were performed to evaluate the functional characteristics of the samples. To measure dark and illuminated currents chrono-amperometric tests were carried out at room temperature under front wall illumination using an Autolab PGSTAT30 potentiostat/galvanostat in a standard three-electrode set-up with a saturated Ag/AgCl reference electrode, a Pt wire as counter and a Ti foil, on which the powder of the samples was deposited, as working electrode. A suspension of ferrite powder, solvent and Carbowax polymer was drop deposited on the Ti foil, dried at 80 °C, and then annealed at 200 °C in air for 3 h to remove the Carbowax polymer from the photoelectrode surface. Sunlight was simulated with a 300 W xenon ozone-free arc-lamp equipped with AM 1.5 G filter at 100 mW/cm^2. Potentiodynamic curves (photo- and dark currents) were obtained under potential scan in the range −1.5 to +1.5 V at a rate of 0.015 V/s for LF and LSFC2010 samples. For all the samples potentiostatic plots were obtained by applying a positive bias of 0.1 V between the photo(working)-electrode and the reference electrode through different ON–OFF irradiation cycles. The selected bias conditions are the same generally used to test the photoelectrochemical properties of photoactive materials such as Degussa P25 titania. 1 M KOH solution purged with N_2 was used as the electrolyte.

Quasi-Fermi levels of electrons were measured according to the literature [14]. 20 mg of the powder were suspended in 100 cm^3 of 0.1 M $NaNO_3$ in the presence of 20 mg of methyl viologen dichloride and irradiated with UV light (medium-pressure Hg lamp Helios Italquartz, Italy). Suspensions were stirred and purged with N_2 prior to and during the measurement. The pH was adjusted by HNO_3 and NaOH solutions and monitored with a pH-meter. In general the starting suspension had pH 1.7 and the experiment was carried out at room temperature. A large surface platinum flag (5 cm^2) and Ag/AgCl were working and reference electrodes, respectively. Stable photovoltages were recorded about 1.5 min after adjusting the pH value.

3. Results and discussion

LF exhibited the orthorhombic symmetry (space group *Pnma*) and crystallized with the well known orthorhombic perovskite structure in agreement with results previously reported for powders prepared at 600 °C [10], and at 900 °C [15]. LSF20 and

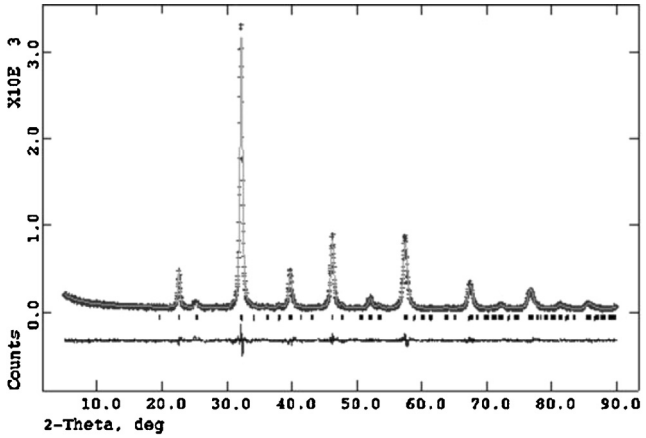

Fig. 1. Observed (cross) and calculated (continuous line) intensities in the XRD pattern of LSFC2010 prepared at 600 °C. The differences between observed and calculated intensities are plotted at the bottom. The crystal structure was refined in the *Pnma* space group.

LSFC2010 perovskites prepared at 600 °C were single phase, and crystallized in the orthorhombic symmetry (in Fig. 1 the XRD data from LSFC2010 are shown). For LSFC2020 sample prepared at 600 °C the reflections were broader and with lower intensity than those of LSFC2010, but no additional peaks were detected in the diffractogram. We have previously reported the structural characterization of samples calcined at 980 °C [11,13]: LSF20 and LSFC2010 powders were monophasic with orthorhombic symmetry, while LSFC2020 was biphasic, with a main (78.5 wt%) orthorhombic phase and a secondary rhombohedral phase. The oxygen content determined by Rietveld refinement of neutron diffraction data resulted in full occupancy of the oxygen sites for both LSFC2010 and LSFC2020 [11]. The unit cell volume decreases with increasing Cu doping. Since the larger Cu^{2+} cation partially substitutes Fe^{3+} cation (Cu^{2+}(VI) = 0.73 Å, Fe^{3+}(VI) = 0.645 Å), a charge compensation mechanism occurs by oxidation of Fe/Cu cations [13].

The morphology of the LF powder is shown in Fig. 2. Agglomerations of particles with particle size smaller than 100 nm are detectable. As reported in Table 1 the partial replacement of lanthanum with strontium and of iron with copper in the system $La_{1-x}Sr_xFe_{1-y}Cu_yO_3$ brought a significant increase in the surface area of the samples measured after annealing at 600 °C. In fact an increase from 14 to 25 m^2/g was observed going from the parent structure of the LF to that of the more substituted LSFC2020.

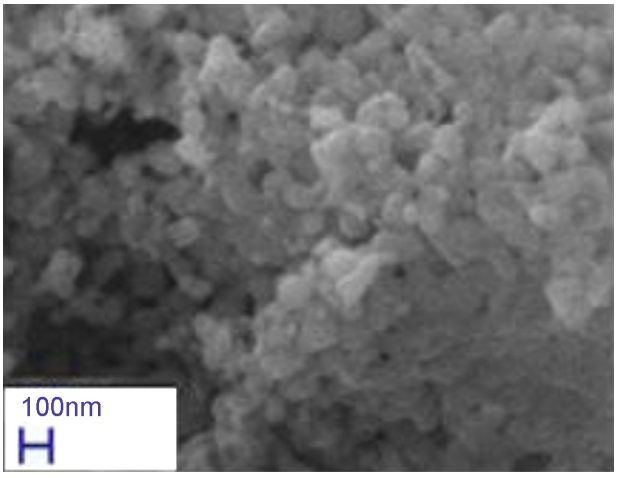

Fig. 2. ESEM micrograph of LF powder calcined at 600 °C.

Table 1
Selected morphological parameters: powder colour, mean crystallite sizes (from XRD data), and BET surface areas for samples calcined at 600 °C.

Samples	LF[a]	LSF20	LSFC2010	LSFC2020
Colour	Ochre	Black	Black	Black
Mean crystallite size (nm)	43	26	22	18
BET surface area (m^2/g)	14	18	23	25

[a] BET surface area of LF prepared at 900 °C is 6 m^2/g.

Correspondingly, crystallite size calculated from XRD data using the Debye Scherrer equation decreases as the Sr/Cu doping increases.

Fig. 3A shows the diffuse reflectance UV–vis spectrum of sample LF calcined at 600 °C. The absorption edge between 400–600 nm was related to the band-gap energy of LF [7]. It was assigned to the transfer of electrons from the valence band (mainly contributed by strongly mixed e_g states of Fe *3d* and O *2p* states) to the conduction band (t_{2g} states of Fe *3d*).

For estimation of the optical band gap E_g Kubelka–Munk function $F(R_\infty)$ of the diffuse reflectance spectra was used instead of the absorption coefficient. As done for $La_{1-x}Ag_xFeO_3$ [16] and $Bi(Fe_{1-x}Mn_x)O_3$ [17] the absorption data were modeled assuming a direct gap by plotting $(F(R_\infty)E)^2$ as a function of E the energy of incident photons. The intercept on abscissa of the $(F(R_\infty)E)^2$ vs E gave the value of optical absorption edge energy. Following this procedure the measured E_g for nanosized LF is 2.54 eV (Table 2), larger than that value previously found for dense polycrystalline sample 2.1 eV [7] and for porous submicrometric powders 2.4 eV [16], but smaller than 2.64 eV estimated using direct transition for epitaxial thin film of LF [18].

In LSF20, LSFC2010 and LSFC2020 the absorption of visible light is higher than in LF in accordance with their black color (the parent LF is ochre in color) (see Fig. 3B). As has been reported in refs [7–9] hole doping via Sr^{2+} for La^{3+} substitution causes changes in the electronic structure introducing hole states at about 1.0 eV above the Fermi energy. It is important to note that even for Sr-content $x = 0.40$ (double than here) the hole states do not overlap the top of the valence band retaining the charge-transfer-type behaviour, although with a minor band-gap energy [8,9].

For LSF20, LSFC2010 and LSFC2020 in addition to the absorption edge between 400 and 600 nm we considered an additional transition found at lower energy (higher wavelength) than the previous transition. Following Refs. [8,9] this transition was attributed to the hole states doped into the band-gap. The energy of the first transition was determined assuming a direct gap and the estimated transition energies are reported in Table 2 for each material. These correspond to 2.2 eV for LSF20, 2.1 eV for LSFC2010, and 2.3 eV for LSFC2020. The substitution of Sr^{2+} for La^{3+} causes a red-shifting of the transition in accordance with a recent work [18].

In agreement with Scafetta et al. [18] the transition found at lower energy likely depicts the true band gap transition. The energy value for this transition was estimated about 0.70 eV for LSF20, LSFC2010 and LSFC2020 (see Fig. 3C).

Fig. 4 reports the current density (J) vs potential (E) curves for the samples LF and LSFC2010 recorded in dark condition and under simulated solar irradiation AM 1.5 G. In both cases it is clearly shown how the photocurrent density recorded by irradiation (red and green curves) is significantly higher than the dark current (black and dark green curves) with mean increases in photocurrent density of about 0.8 mA/cm^2 for LF and 2.9 mA/cm^2 for LSFC2010, respectively for potential values >1 V, whereas values of about some microamperes per cm^2 were observed at lower potential (around 0.1 V) as discussed below and well illustrated in chronoamperometric plots reported in Figs. 5 and 6. It is worth to note that the plots do not show a proper plateau region. In order to check a possible contribution from the Ti substrate (for example due to the formation of titanium dioxide) a blank experiment was performed using the Ti foil annealed at 200 °C in air for 3 h, without the pasted ferrite layers. As expected no photocurrent was measured in accordance with the fact that the production of TiO_2 by oxidizing the surfaces of Ti foils requires a thermal treatment in air at temperatures higher than 400 °C [19]. Further investigations are required to check the effects of the porosity of the ferrite layers on the current density.

As concerns the potentiostatic plots by photo-irradiation with UV–vis light a rapid generation of photocurrent was observed when the electrons photogenerated by the materials were captured and transported on the Ti foil (Fig. 5). All the samples were found to be photoactive and a gradual reduction of the photocurrent was observed when the tests were conducted with the aid of filters capable of blocking increasing ranges of the incident UV radiation (see Fig. 6). The results show that the LF sample calcined at 600 °C exhibits the highest activity, and the activity decreases with increasing calcination temperature, which is in good agreement with the surface area measurements, indicating lower activity for the samples with smaller surface area. The observed photocurrent response was significantly different depending on the composition of the samples, with a higher density of photocurrent for LF compared to that recorded for the samples with partial substitution of lanthanum and iron in the structure. Furthermore ON/OFF illumination of the materials deposited on the photoelectrode shows an instantaneous rise in photocurrent and quick recovery to the original photocurrent density through multiple ON/OFF cycles. The monitoring during discontinuous illumination revealed stability and reproducibility of the photocurrent density in all the tested samples (see Fig. 7).

Quasi-Fermi levels of electrons, E_{fb}, were measured according to the literature [14] by measuring the photovoltage as a function of pH value. For this purpose a slurry electrode consisting of 20 mg of the powder, suspended in 100 cm^3 of 0.1 M $NaNO_3$ in the presence of 20 mg of methyl viologen dichloride (MV^{2+}) was irradiated with UV light (medium-pressure Hg lamp Helios Italquartz, Italy). Increasing the pH value of the suspension shifts the edges of the conduction and valence bands towards more negative potentials so that, approaching the inflection point pH_0, photogenerated electrons can reduce MV^{2+} present into the solution to its corresponding radical cation. A lower pH_0 value corresponds to a more negative quasi-Fermi level. From pH_0 value of the corresponding

Table 2
The quasi-Fermi level E_{fb}, and the optical band gap E_g for samples calcined at 600 °C (LF, LSF20, LSFC2010 and LSFC2020) and calcined at 980 °C (LSF20, LSFC2010). The value of optical absorption edge energy was obtained by extrapolating to zero a linear fit to a plot of $(F(R_\infty)E)^2$ vs E.

Samples	LF 600 °C	LSF20 600 °C	LSF20 980 °C	LSFC2010 600 °C	LSFC2010 980 °C	LSFC2020 600 °C
E_g (eV)	2.54	0.7	–	0.7	0.8	0.7
E_{fb1} (V)	−0.63	−0.62	−0.63	−0.65	−0.67	−0.63
E_{fb2} (V)	–	–	–	−0.56	–	−0.56

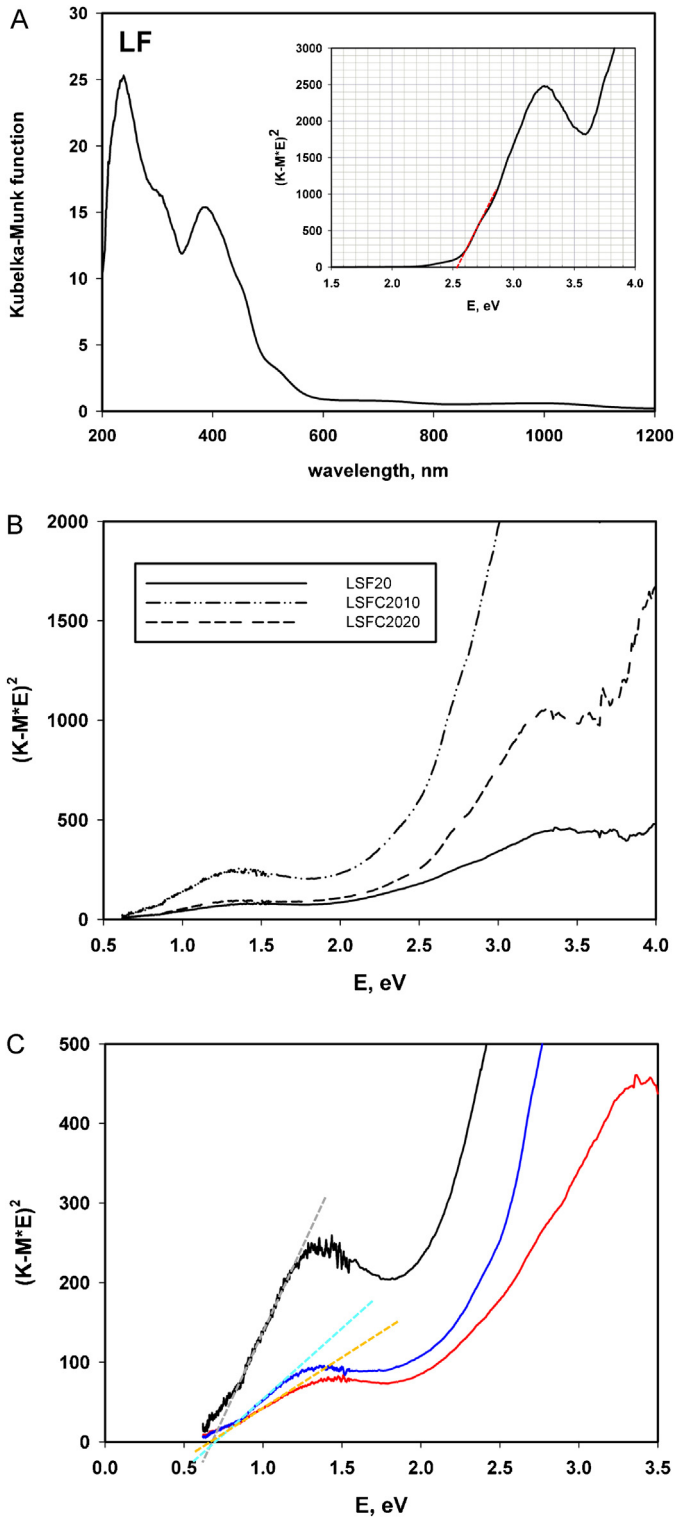

Fig. 3. UV–vis absorption spectra of LF (A) and LSF20, LSFC2010 and LSFC2020 (B and C) calcined at 600 °C.

titration curve (see Fig. 8), the quasi-Fermi level at pH 7 can be calculated via the following equation:

$$E_{fb}(pH) = E^{\circ}_{MV^{2+}/MV^{+}} + k(pH_0 - pH)$$

where $E^{\circ}_{MV^{2+}/MV^{+}}$ is the redox potential of the MV^{2+}/MV^{+} couple and k is assumed to be equal to 0.059 V. The obtained values are reported in Table 2.

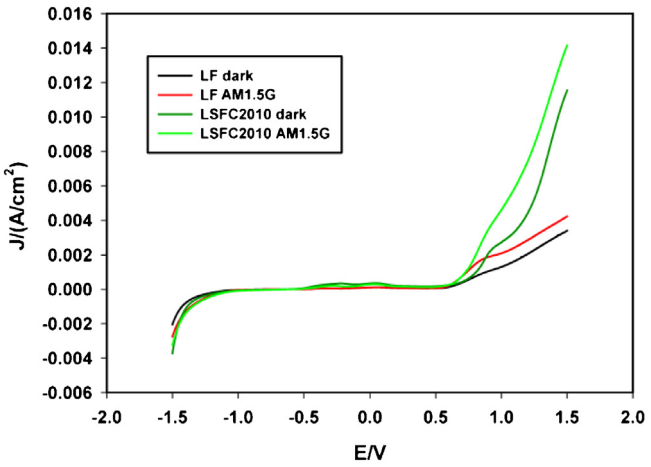

Fig. 4. Potentiodynamic plots (photocurrent density (J) versus applied potential (E)) of LF and LSFC2010 samples recorded in the dark (black and dark green lines) and under light radiation (red and light green lines) at scan rate 0.015 V/s. The photoactivity was examined under AM 1.5G (100 mW/cm^2) simulated solar irradiation in 1 M KOH electrolyte with a Pt wire and Ag/AgCl as the counter and the reference electrodes, respectively. (For interpretation of the references to colour in this figure legend, the reader is referred to the web version of the article.)

Fig. 8 reports the measurements carried out with the sample LSFC2010 prior to (A1) and after (A2) calcination at 980 °C and with the sample LSF20 prior to (B1) and after (B2) calcination at 980 °C. Sample LSFC2020 (not shown) showed a titration curve similar to that in Fig. 8A1 whereas samples without copper behave analogously to Fig. 8B1 (not shown).

It should be pointed out that the present method for determining the quasi-Fermi level can be successfully used for both p-type and n-type semiconductors. In fact, semiconductor irradiation of suitable energy causes the formation of two quasi-Fermi levels (one for the holes and one for the electrons) and the method in both cases gives information about the potentials of the photogenerated electrons. By assuming that the difference between the quasi-Fermi level potential and the conduction band edge is negligible, the valence band edge values are obtained by addition of the band gap energies reported in Table 2.

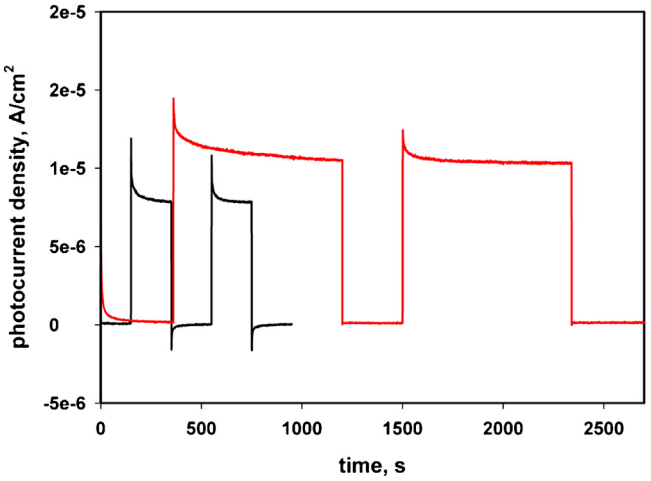

Fig. 5. Photocurrent profiles of LSFC2010 and LF samples; black line and red line, respectively. Both sample were calcined at 600 °C and deposited on a Ti metal support. The potential of the KCl saturated Ag/AgCl reference electrode was E° = 0.197 V vs SHE at 25 °C. ON–OFF cycles with different interval time for a better visualization of the trends were carried out. Irradiation was conducted by a 300 W Xe light source. (For interpretation of the references to colour in this figure legend, the reader is referred to the web version of the article.)

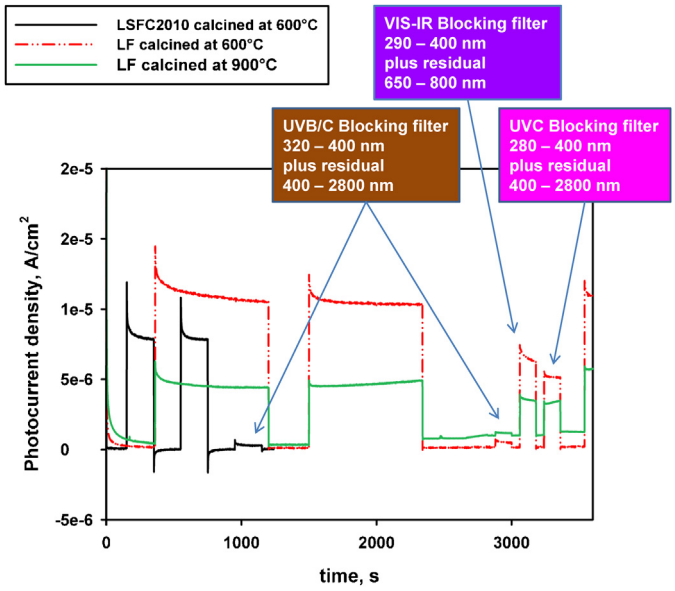

Fig. 6. Typical photocurrent profiles of LF (calcined at 600 °C and 900 °C), and LSFC2010 (calcined at 600 °C) recorded under illumination with a 300 W Xe light source with (or without) blocking filters used to cut different fractions of incident light. The potential of the KCl saturated Ag/AgCl reference electrode was E° = 0.197 V vs SHE at 25 °C.

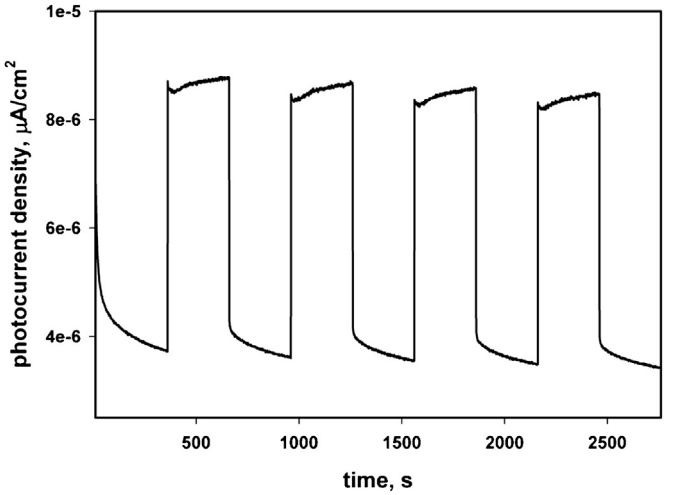

Fig. 7. Typical photocurrent response of a LF film (activated at 900 °C and deposited on Ti metal support) to ON–OFF cycles carried out by means of a 300 W Xe light source. The potential of the KCl saturated Ag/AgCl reference electrode was E° = 0.197 V vs SHE at 25 °C.

It may be noted that the position of the quasi-Fermi level for all the catalysts is about the same within experimental error (between −0.62 and −0.67 V). The presence of strontium did not influence the flat band potential of the powders. On the other hand, the presence of copper caused an important and reproducible change in the titration curve as shown in Fig. 8. In fact, at about pH 4.5 the curve slope suddenly changes indicating that, from this pH value, an electron transfer can take place from a different phase or a different semiconducting material present into the powder to the MV^{2+} dissolved into the suspension. This feature was observed only when copper was present into the powders *i.e.* for LSFC2010 and for LSFC2020. Rusina et al. [20] observed a similar behaviour

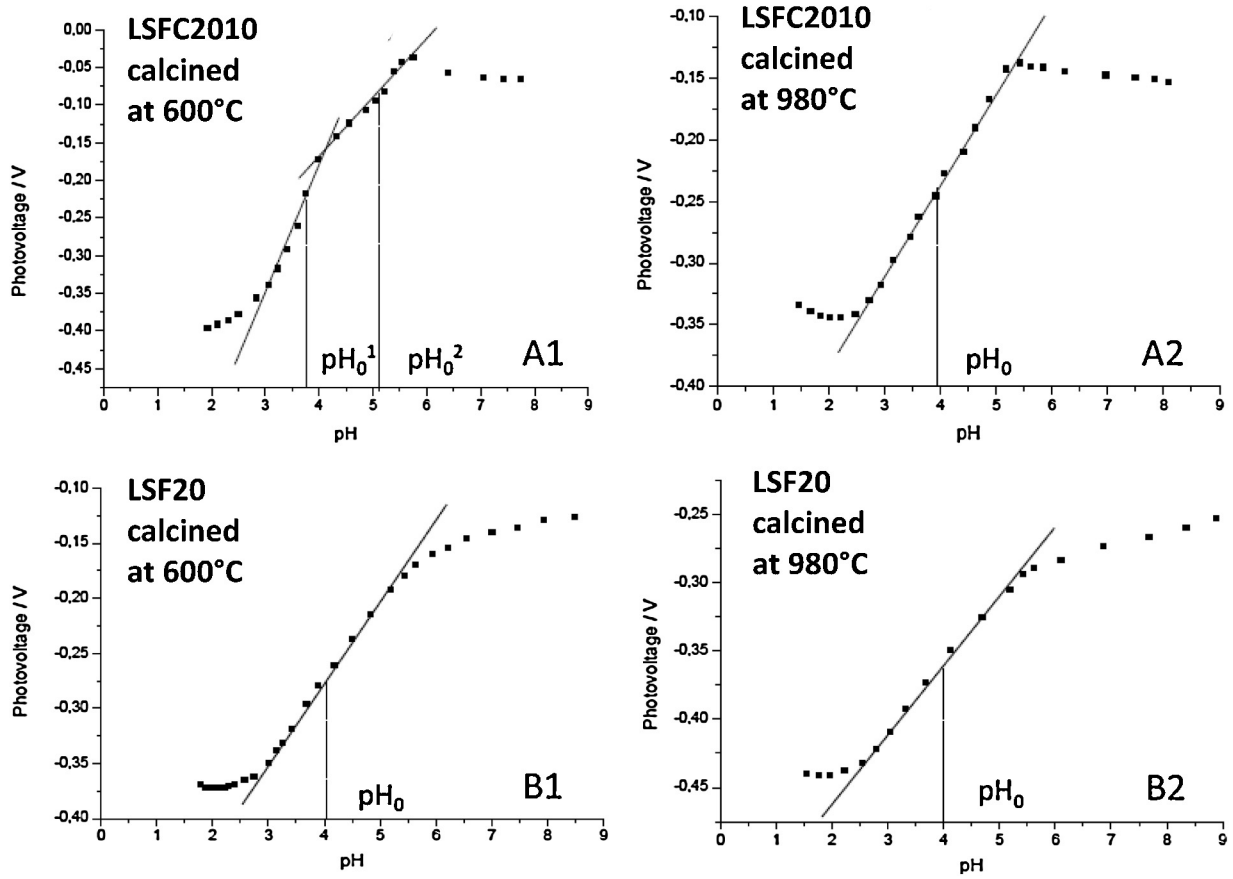

Fig. 8. Variation of photovoltage with pH value. 20 mg of catalyst with 20 mg of methyl viologen dichloride are suspended in 100 mL of 0.1 M $NaNO_3$ aqueous solution at room temperature. Pt, working electrode and Ag/AgCl, reference electrodes.

for mixed semiconductors titanium dioxide–iron titanate. This finding suggests that Cu-doping promotes the presence into the powders calcined at 600 °C of a secondary phase with different electronic properties. Although the XRD analysis did not suggest the presence of a secondary phase for LSFC2010 and LSFC2020 powders calcined at 600 °C the Rietveld refinements gave unsatisfactory agreement factors, so a certain structural disorder and/or lack of homogeneousness could not be excluded. Moreover, the calcination at 980 °C of the Cu-containing samples resulted in the disappearance of this specific feature, leaving a powder with the same flat band potential as the others listed in Table 2. Interestingly, calcining at the same temperature the Cu-undoped samples (LF and LSF20) did not produce changes in the titration curve. For samples calcined at 980 °C detailed NPD analyses [11] have shown that LSFC2010 is monophasic, while LSFC2020 is largely biphasic, so it is unlikely that the change in the titration curve is due to the disappearance of a secondary phase after calcining at 980 °C. It has been reported that in the system $La_{1-x}Sr_xFeO_{3-w}$ the higher the calcining temperature the lower are the concentration of oxygen vacancy and the content of iron cations with oxidation state larger than +3 [21]. Accordingly, the NPD analysis has indicated a full occupancy of the oxygen sites in LSFC2010 and LSFC2020 calcined at 980 °C [11]. Possibly the thermal treatment at 980 °C causes a good bulk and surface chemical homogeneousness in Cu-containing samples. In general, doping with copper may lower the temperature during the auto-combustion synthesis, as found for the system $LaFe_{1-y}Cu_yO_{3-w}$ [10]. However further investigations are necessary to clarify this point.

The extent of photocurrent obtained in the case of Cu-doped powders was lower with regard to that obtained by using copper-free powders. This finding is in good agreement with the results of the quasi-Fermi level measurements, *i.e.* with the presence of intermediate energy states introduced when Cu was present in the powders. Being these states at lower energy than the primary Fermi level of the powders, recombination of the photoproduced excitons and lowering of the photocurrent response are more likely.

4. Conclusions

All samples showed moderate absorbance of visible light. All powders showed photocurrent response; the highest photocurrent was obtained for LF calcined at 600 °C.

In order to elucidate the complex electronic properties of these samples, the quasi-Fermi levels of electrons were measured and the results indicate that: (i) the position of the quasi-Fermi level for all the photocatalysts calcined in the range 600–980 °C is about the same within experimental error (between −0.62 and −0.67 V), (ii) doping with strontium does not influence the flat band potential of the powders, and (iii) for LSFC2010 and LSFC2020 the presence of copper caused an important and reproducible change in the titration curve, indicating the presence of intermediate energy states in the samples calcined at 600 °C, but not in those calcined at 980 °C. Further work will be required to ascertain whether an intermediate temperature structural transition takes place, and to investigate a possible photocatalytic activity for removal of organic molecules present in air or water effluents. Based on these photoelectrochemical characteristics, the proposed perovskite-type lanthanum powders could be considered not only as traditional electrodes for high temperature solid oxide fuel cells (SOFC) but also as functional inorganic materials in photocatalytic applications operating at low temperature.

Acknowledgements

The initial part of the work has been financially supported by INSTM and Regione Lombardia within the frame of the project "Nanostructured catalysts for energy and environment". Thanks to Ivan Grigioni for technical assistance.

References

[1] T. Ohno, T. Tsubota, Y. Nakamura, K. Sayama, Preparation of S, C cation-codoped $SrTiO_3$ and its photocatalytic activity under visible light, Applied Catalysis A: General 288 (2005) 74.
[2] V. Augugliaro, M. Litter, L. Palmisano, J. Soria, The combination of heterogeneous photocatalysis with chemical and physical operations: a tool for improving the photoprocess performance, Journal of Photochemistry and Photobiology C: Photochemistry Reviews 7 (2006) 127.
[3] D.F. Wang, T. Kako, J.H. Ye, Efficient photocatalytic decomposition of acetaldehyde over a solid-solution perovskite $(Ag_{0.75}Sr_{0.25})(Nb_{0.75}Ti_{0.25})O_3$ under visible-light irradiation, Journal of the American Chemical Society 130 (2008) 2724.
[4] H. Su, L. Jing, K. Shi, C. Yao, H. Fu, Synthesis of large surface area $LaFeO_3$ nanoparticles by SBA-16 template method as high active visible photocatalysts, Journal of Nanoparticle Research 12 (2010) 967.
[5] G. Centi, S. Perathoner, Problems and perspectives in nanostructured carbon-based electrodes for clean and sustainable energy, Catalysis Today 150 (2010) 151.
[6] I. Wærnhus, P.E. Vullum, R. Holmestad, T. Grande, K. Wiik, Electronic properties of polycrystalline $LaFeO_3$. Part I: experimental results and the qualitative role of Schottky defects, Solid State Ionics 176 (2005) 2783.
[7] T. Arima, Y. Tokura, J.B. Torrence, Variation of optical gaps in perovskite-type *3d* transition-metal oxides, Physical Review B 48 (1993) 17006.
[8] A. Chainani, M. Mathew, D.D. Sarma, Electronic structure of $La_{1-x}Sr_xFeO_3$, Physical Review B 48 (1993) 14818.
[9] H. Wadati, D. Kobayashi, H. Kumigashira, K. Okazaki, T. Mizokawa, A. Fujimori, K. Horiba, M. Oshima, N. Hamada, M. Lippmaa, M. Kawasaki, H. Koinuma, Hole-doping-induced changes in the electronic structure of $La_{1-x}S_xFeO_3$: soft X-ray photoemission and absorption study of epitaxial thin films, Physical Review B 71 (2005) 035108.
[10] T. Caronna, F. Fontana, I. Natali Sora, R. Pelosato, Chemical synthesis and structural characterization of the substitution compound $LaFe_{1-x}Cu_xO_3$ ($x = 0 - 0.40$), Materials Chemistry and Physics 116 (2009) 645.
[11] I. Natali Sora, T. Caronna, F. Fontana, C. De Julián Fernández, A. Caneschi, M. Green, Crystal structures and magnetic properties of strontium and copper doped lanthanum ferrites, Journal of Solid State Chemistry 191 (2012) 33.
[12] A. Cavalieri, T. Caronna, I. Natali Sora, J.M. Tulliani, Electrical characterization of room temperature humidity sensors in $La_{0.8}Sr_{0.2}Fe_{1-x}Cu_xO_3$ ($x = 0$, 0.05, 0.10), Ceramics International 38 (2012) 2865.
[13] I. Natali Sora, T. Caronna, F. Fontana, C. de Julián Fernández, A. Caneschi, M. Green, P. Bonville, Charge compensation and magnetic properties in Sr and Cu doped La–Fe perovskites, EPJ Web of Conferences 40 (2013) 15005.
[14] A.M. Roy, G.C. De, N. Sasmal, S.S. Bhattacharyya, Determination of the flat-band potential of semiconductor particles in suspension by photovoltage measurement, International Journal of Hydrogen Energy 20 (1995) 627.
[15] H. Falcon, A.E. Goeta, G. Punte, R.E. Carbonio, Crystal structure refinement and stability of $LaFe_xNi_{1-x}O_3$ solid solutions, Journal of Solid State Chemistry 133 (1997) 379.
[16] M.B. Bellakki, B.J. Kelly, V. Manivannan, Synthesis, characterization, and property studies of $(La,Ag)FeO_3$ ($0.0 \le x \le 0.3$), Journal of Alloys and Compounds 489 (2010) 64.
[17] X.S. Xu, J.F. Ihlefeld, J.H. Lee, O.K. Ezekoye, E. Vlahos, R. Ramesh, V. Gopalan, X.Q. Pan, D.G. Schlom, J.L. Musfeldt, Tunable band gap in $Bi(Fe_{1-x}Mn_x)O_3$ films, Applied Physics Letters 96 (2010) 192901.
[18] M.D. Scafetta, Y.J. Xie, M. Torres, J.E. Spanier, S.J. May, Optical absorption in epitaxial $La_{1-x}Sr_xFeO_3$ thin films, Applied Physics Letters 102 (2013) 081904.
[19] L. Özcan, S. Yurdakal, V. Augugliaro, V. Loddo, S. Palmas, G. Palmisano, L. Palmisano, Photoelectrocatalytic selective oxidation of 4-methoxybenzyl alcohol in water by TiO_2 supported on titanium anodes, Applied Catalysis B: Environmental 132–133 (2013) 535.
[20] O. Rusina, W. Macyk, H. Kisch, Photoelectrochemical properties of a dinitrogen-fixing iron titanate thin film, Journal of Physical Chemistry B 109 (2005) 10858.
[21] A. Wattiaux, J.C. Grenier, M. Pouchard, P. Hagenmuller, Electrolytic oxygen evolution in alkaline-medium on $La_{1-x}Sr_xFeO_{3-y}$ perovskite-related ferrites. II: Influence of bulk properties, Journal of The Electrochemical Society 134 (1987) 1718.